Consiglio Nazionale delle Ricerche
Istituto di Matematica Applicata
e Tecnologie Informatiche
“Enrico Magenes”

REPORT SERIES

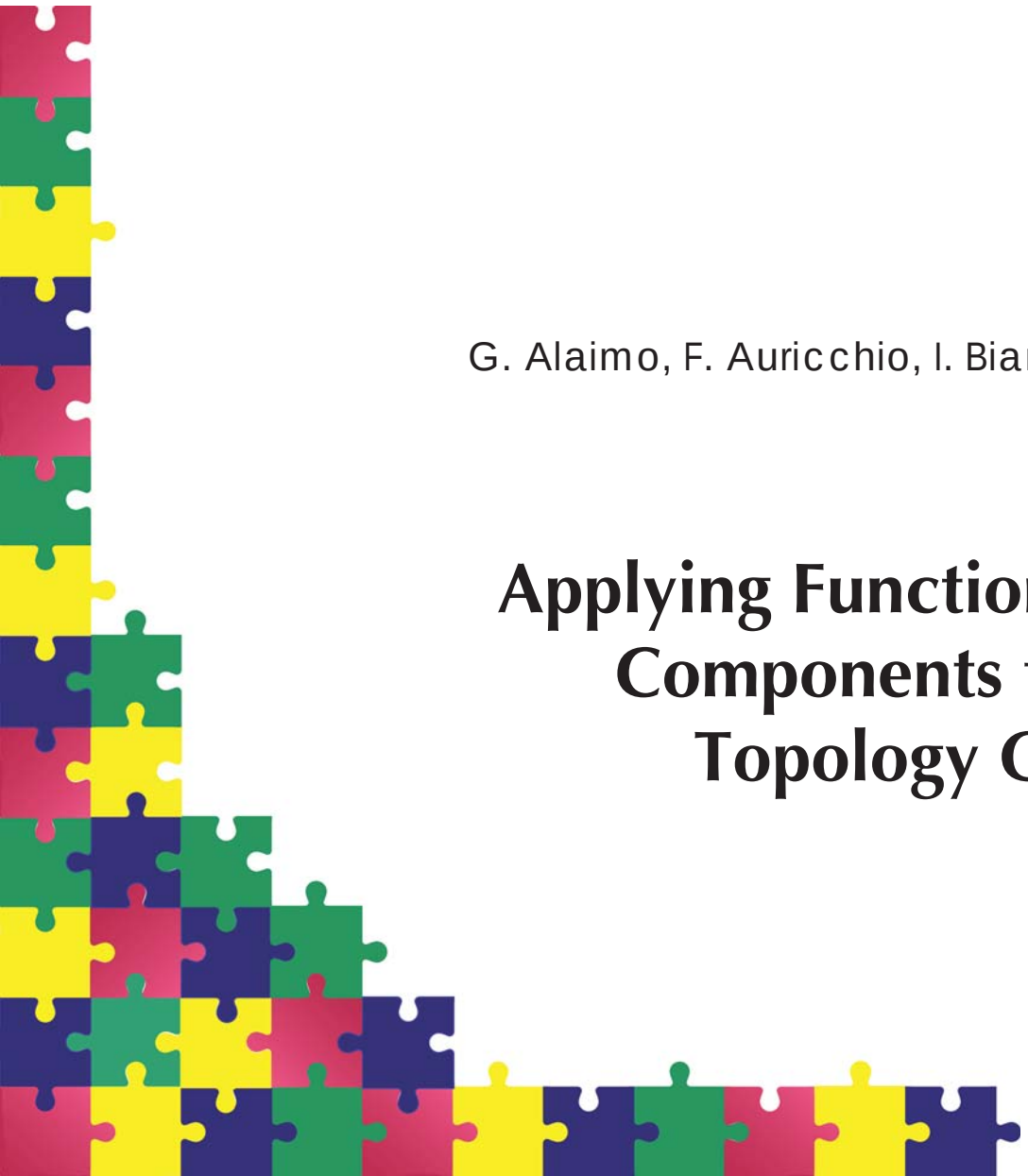

G. Alaimo, F. Auricchio, I. Bianchini, E. Lanzarone

Applying Functional Principal Components to Structural Topology Optimization

17-09

IMATI REPORT Series

Nr. 17-09
April 2017

Editorial Office
Istituto di Matematica Applicata e Tecnologie Informatiche "*E. Magenes*"
Consiglio Nazionale delle Ricerche
Via Ferrata, 5/a
27100 PAVIA (Italy)
Email: reports@imati.cnr.it
http://www.imati.cnr.it

IMATI Report Series Nr. 17-09
April 7, 2017

Applying Functional Principal Components to Structural Topology Optimization

Gianluca Alaimo, Ferdinando Auricchio, Ilaria Bianchini, Ettore Lanzarone

Corresponding author:
Ettore Lanzarone
Istituto di Matematica Applicata e Tecnologie Informatiche “E. Magenes” – CNR
Via A. Corti,12 - 20133 Milano
e-mail address: ettore.lanzarone@cnr.it

Gianluca Alaimo
Dipartimento di Ingegneria Civile e Architettura, Università di Pavia
Via Ferrata, 3 - 27100 Pavia
e-mail address: gianluca.alaimo01@ateneopv.it

Ferdinando Auricchio
Dipartimento di Ingegneria Civile e Architettura, Università di Pavia
Via Ferrata, 3 - 27100 Pavia
e-mail address: auricchio@unipv.it

Ilaria Bianchini
Dipartimento di Matematica, Politecnico di Milano
via Bonardi 9 - 20133 Milano
e-mail address: ilaria.bianchini@polimi.it

Abstract

Structural Topology Optimization optimizes the mechanical performance of a structure while satisfying some functional constraints. Nearly all approaches proposed in the literature are iterative, and the optimal solution is found by repeatedly solving a Finite Elements Analysis (FEA). It is thus clear that the bottleneck is the high computational effort, as these approaches require solving the FEA a large number of times. In this work, we address the need for reducing the computational time by proposing a reduced basis method that relies on the Functional Principal Component Analysis (FPCA). The methodology has been validated considering a Simulated Annealing approach for the compliance minimization in a variable thickness cantilever sheet. Results show the capability of FPCA to provide good results while reducing the computational times, i.e., the computational time for a FEA analysis is about one order of magnitude lower in the reduced FPCA space.

Keywords: *Structural Topology Optimization; Functional Principal Components Analysis; Finite Element Analysis*

[page left intentionally blank]

Applying Functional Principal Components to Structural Topology Optimization

Gianluca Alaimo[1], Ferdinando Auricchio[1],
Ilaria Bianchini[2], Ettore Lanzarone[3*]

[1]Università di Pavia, Department of Civil Engineering and Architecture, Pavia, Italy.
[2]Politecnico di Milano, Department of Mathematics, Milan, Italy
[3]CNR-IMATI, Milan, Italy

Abstract

Structural Topology Optimization optimizes the mechanical performance of a structure while satisfying some functional constraints. Nearly all approaches proposed in the literature are iterative, and the optimal solution is found by repeatedly solving a Finite Elements Analysis (FEA). It is thus clear that the bottleneck is the high computational effort, as these approaches require solving the FEA a large number of times. In this work, we address the need for reducing the computational time by proposing a reduced basis method that relies on the Functional Principal Component Analysis (FPCA). The methodology has been validated considering a Simulated Annealing approach for the compliance minimization in a variable thickness cantilever sheet. Results show the capability of FPCA to provide good results while reducing the computational times, i.e., the computational time for a FEA analysis is about one order of magnitude lower in the reduced FPCA space.

Keywords
Structural Topology Optimization; Functional Principal Components Analysis; Finite Element Analysis.

[*]**Corresponding author:**
Ettore Lanzarone
ettore.lanzarone@cnr.it

1. Introduction

Structural optimization techniques aim to obtain optimized performance from a structure while satisfying several functional constraints, e.g., the total mass to employ or stress limits. The need for optimized solutions in structural applications has increased over the years and has become nowadays fundamental, due to the limited availability of commodities, the environmental impact, the market competition, and the new manufacturing processes, e.g., the 3D-printing.

Three main categories can be distinguished in the wide class of structural optimization methodologies, i.e. *size* optimization, *shape* optimization and *topology* optimization. We focus on the Structural Topology Optimization (STO) of continuum structures, whose aim is to produce an optimized structural component by determining its best mass or volume distribution in a given design domain. Differently from the other alternatives, which deal with predefined configurations, STO design can attain any shape within the domain.

STO is essentially treated as a constrained minimization or maximization problem. Several approaches and algorithms have been proposed for STO, as documented by the huge literature available on the topic (Huang & Xie, 2010; Hassani & Hinton, 2012; Bendsøe & Sigmund, 2013; Sigmund & Maute, 2013; Van Dijk et al., 2013; Rozvany & Lewiński, 2014; Rozvany, 2014). The main distinction is between gradient-based and non-gradient-based approaches; however, nearly all of the algorithms are iterative, and the optimal solution is found by repeatedly performing a structural Finite Elements Analysis (FEA) which involves the solution of the equilibrium equations of the problem under study.

On the one hand, such iterative approaches are powerful, as they allow to determine optimized solutions in a variety of situations without additional assumptions. On the other hand, the bottleneck of such approaches is the high computational effort, as they require to perform the FEA a large number of times, as reported in Bendsøe & Sigmund (2013). As an example, in a minimum compliance problem (see Sect. 2.1), up to the 97% of the total computational time may be employed in the numerical solution of the equilibrium equations (Borrvall & Petersson, 2001).

In this perspective, the need for reducing the computational time of performing the FEA instances in STO, especially for large problems and 3D applications, is crucial. In this work, we address this issue by proposing a reduced basis method that relies on the Functional Principal Component Analysis (FPCA), namely the functional counterpart of the classical Principal Component Analysis (PCA), in order to improve the efficiency of the FEA employed in STO.

Coupling FPCA with structural FEA allows to reduce the dimensionality of the structural problem, i.e., the number of equilibrium equations to be solved. In this way, a substantial saving of the computational time required could be achieved at each iteration, without any appreciable loss of accuracy. Thus, the advantages in terms of time reduction for STO could

be relevant.

To the best of our knowledge, the idea of coupling FPCA and FEA has been exploited only once in the literature (Bianchini et al., 2015). However, in the cited reference, the authors coupled FPCA and FEA for the purpose of uncertainty quantification, in order to estimate the probability distribution of some output random variables (e.g., the displacement in a given direction) in the presence of stochastic input parameters (e.g., the Young modulus). The novelty of the present work is to couple FPCA and FEA for an optimization purpose, which has been never considered before.

Briefly, at each iteration of the STO, we convert the FEA problem into a reduced one by projecting into a smaller space by means of a data-driven reduced FPCA basis. The reduced problem is solved and, if the error associated with the solution is below a given threshold, the *reduced* solution is accepted; otherwise, the original FEA problem is solved and the *complete* solution is also used for updating the FPCA basis.

In the present work, we employ the proposed methodology along with a Simulated Annealing (SA) approach, as an example of iterative non-gradient based algorithm. However, we underline that the proposed FPCA methodology can be used along with any iterative algorithm employed in STO. More in general, the discussion on the most suitable algorithm for STO is still open (Sigmund, 2011); anyway, this is not the focus of our work.

The paper is structured as follows. A literature review on STO and the approaches to reduce the dimensionality and the computational effort in FEA is presented in Sect. 2. The considered problem and the proposed methodology are described in Sect. 3. Then, the test case used to validate the approach is shown in Sect. 4, while the computational analyses and the related results are presented in Sect. 5. The discussions and the conclusion of the work are finally drawn in Sect. 6.

2. Literature review

2.1. Structural Topology Optimization (STO)

As highlighted in Sect. 1, a huge literature on STO is available regarding theoretical aspects, numerical methods and applications.

Collections of lectures dealing with several aspects of STO and optimality criteria are edited by Rozvany & Lewiński (2014) and Rozvany (2014). Review papers focusing on level-set methods, evolutionary approaches and established methods of structural topology optimization are also available (Rozvany, 2009; Huang & Xie, 2010; Sigmund & Maute, 2013; Van Dijk et al., 2013). The fundamentals of the material distribution method and its extension to anisotropic materials are presented in Bendsøe & Sigmund (2013), considering dynamic and buckling problems as well as the design of truss structures. Hassani & Hinton (2012) treated STO with periodic material distribution, for which macro constitutive models are derived through suitable homogenization techniques.

A widely used methodology in STO is represented by the density based approach, in which the design domain Ω is discretized into a set of N elements and the density parameters ρ_i associated to each element i ($i = 1, \ldots, N$) are optimized. This method gained popularity because it does not require domain re-meshing at each iteration (Zegard & Paulino, 2016).

Following this approach, the elastic modulus E_i of element i is related to its density ρ_i according to the modified Solid Isotropic Material with Penalization (SIMP) scheme as follows (Bendsøe, 1989; Zhou & Rozvany, 1991; Sigmund, 2007):

$$E_i(\rho_i) = E_{min} + \rho_i^p (E_0 - E_{min}), \qquad \forall i \tag{1}$$

where E_0 is the elastic modulus of the solid material, E_{min} is the lower limit of the elastic modulus (introduced to overcome computational issues in the presence of zero-stiffness elements while solving the equilibrium equations), $\rho_i \in [0, 1]$, and $p \geq 1$ is a penalization factor. Higher values of p make less convenient to use intermediate values of density between solid ($\rho_i = 1$) and void ($\rho_i = 0$).

SIMP method with no penalization ($p = 1$) yields a linear relation between E_i and ρ_i, giving the so-called *variable thickness sheet problem* for which the solution is unique in the case of stiffness maximization (Petersson, 1999).

Discrete elements i for STO usually coincide with the mesh used for numerically solving the FEA problem, even though they are theoretically independent. As a consequence, the optimized solution depends on the level of the mesh refinement. Indeed, the introduction of finer meshes (and consequently of smaller elements in a structure with fixed domain) leads to a material distribution in the form of micro-structure, which increases the efficiency of the optimized structure. In fact, microstructure-like material distributions lead to an improved use of the material. However, even though a fine mesh is required to properly solve the FEA problem, it is not always possible to build features below a certain scale from a technical feasibility viewpoint.

To overcome this issue, relaxation or restriction methods can be used to uncouple the discretization into elements from the mesh(Bendsøe & Kikuchi, 1988; Ambrosio & Buttazzo, 1993; Haber et al., 1996; Sigmund, 1997; Bourdin, 2001; Bruns & Tortorelli, 2001; Xu et al., 2010). The rationale behind these methods is the reduction of the space of the admissible designs by imposing weak constraints or restrictions on the density variation; thus, material configurations resembling micro structures can be avoided.

2.2. Dimensionality reduction in FEA

Dimensionality reduction in FEA is based on spectral decomposition of the covariance/correlation structure of the displacement field $\boldsymbol{u}(\boldsymbol{x}, \boldsymbol{\rho})$, where $\boldsymbol{x}$ denotes the coordinates of a point in the considered domain Ω and $\boldsymbol{\rho}$ represents a vector of parameters, e.g., densities, characterizing the FEA instance at each given iteration of the STO optimization.

Spectral methods are widely adopted in the literature (Ghanem & Spanos, 1991). Among them, PCA and Karhunen-Loève expansion are those frequently applied to FEA; the first considers the covariance matrix, while the latter the spectrum of the correlation matrix. Both of them require the knowledge of the covariance structure of $\boldsymbol{u(x, \rho)}$, and in particular of the corresponding eigenfunctions. The covariance structure is estimated from a set of already available solutions of the FEA problem, i.e., the basis depends on the covariance function of the solution process and the approach is *data dependent*.

Alternatively, the Proper Generalized Decomposition (PGD) represents an *a priori approach*, which does not rely on previous FEA solutions (Nouy, 2010; Chinesta et al., 2011). Indeed, the solution is approximated *a priori* by minimizing a norm of the error with respect to the Karhunen-Loève decomposition, leading to a pseudo eigenproblem (details can be found in Chinesta et al. (2013)).

Finally, there exist other well-established methods in the literature, based on alternative expansions, which involve a basis of known random functions with deterministic coefficients, namely the Polynomial Chaos Expansion (PCE). The latest methodological developments of PCE can be found in Panayirci & Schuëller (2011) and Yu et al. (2012), while recent applications can be found in different fields, e.g., hydrology (Sochala & Le Maître, 2013), piezoelectric materials (Umesh & Ganguli, 2013), and dosimetry to study the human exposure to magnetic fields (Liorni et al., 2014).

Resuming PCA, it is widely used in statistics to look at the covariance structure of multivariate and complex data (Johnson & Wichern, 1992; Ramsay & Silverman, 2005). In the context of mechanical systems, the method turns out to be useful for characterizing the dynamic behavior and to reduce the order of linear and non-linear systems (Kerschen et al., 2005). Thus, PCA has been successfully applied in a variety of problems, e.g., aeroelastic problems, damage detection, dynamic characterization, and modal analysis. It was initially applied in solid mechanics (Sirovich, 1987); then, it has been employed in structural nonlinear dynamics (Dulong et al., 2007) and to analyze vibro-impact systems (Ritto et al., 2012).

In particular, in Dulong et al. (2007), PCA has been employed for real-time analysis of non-linear mechanical behaviors. Interestingly for our work, the approach is divided into a training phase and a real-time phase. In the training phase, several FEA solutions are computed under different load values; then, PCA is used in the real-time phase to reduce the amount of data to store and the computational time.

Moreover, it is worth mentioning that, in the context of stochastic FEA, Florentin & Díez (2012) introduced an adaptive strategy to build a reduced basis in which, at each Monte Carlo iteration, the distance between the FEA solution and the solution obtained in the reduced space is checked. If the distance is larger than a threshold, the reduced solution is discarded and the complete solution is computed and added to the current basis. Their proposed approach measuring the distance between the solutions is interesting; however, the

adopted reduced basis is not orthogonal, thus leading to an ill-conditioned matrix for the basis change.

All of the works in which the decomposition exploits the covariance matrix are based on the standard PCA, where data are treated as multivariate vectors, thus merely considering the displacements of the nodes of the mesh. On the contrary, the FPCA (Ramsay & Silverman, 2005; Horváth & Kokoszka, 2012) has been only adopted in Bianchini et al. (2015), to build the reduced basis in the context of stochastic FEA. The approach in Bianchini et al. (2015) relies on the idea of evaluating the distance between the complete FEA solution and the solution obtained in the reduced space to assess whether to keep or to discard a reduced solution (as in Florentin & Díez (2012)); however, a data-driven basis is built according to the FPCA.

To conclude, PCA has been already adopted in the literature to address optimization problems (an overview of several optimization problems related to PCA under various geometric perspectives can be found in Reris & Brooks (2015)). However, to the best of our knowledge, the functional counterpart (FPCA) that we are here proposing has been never coupled with FEA in the context of structural optimization, and only once in the context of stochastic FEA (Bianchini et al., 2015).

3. Proposed methodology

We first describe in Sect 3.1 the addressed STO problem; then we present the approach proposed to solve such a problem. The core of the approach (i.e., FPCA applied to FEA) is detailed in Sect. 3.2, while the iterative SA algorithm for this case is presented in Sect. 3.3. Finally, precautions to take for properly employing the FPCA basis are highlighted in Sect. 3.4.

3.1. Addressed problem

We refer to a linear elastic structural problem in a continuous domain Ω, whose goal is to find the displacement field $\boldsymbol{u}(\boldsymbol{x}) \in L^2(\Omega)$ that minimizes the overall elastic energy (or compliance) $\widehat{C}$, which depends on the displacement $\boldsymbol{u}(\boldsymbol{x})$ as follows:

$$\widehat{C} = \frac{1}{2} \int_{\Omega} \boldsymbol{f}(\boldsymbol{x}) \, \boldsymbol{u}(\boldsymbol{x}) \, d\boldsymbol{x} \tag{2}$$

where $\boldsymbol{f}(\boldsymbol{x})$ is the imposed force field.

We consider the variable thickness sheet problem (see Sect. 2.1). We discretize the domain into elements i ($i = 1, \ldots, N$) with the same area, and each elastic modulus E_i linearly depends on the density ρ_i as $E_i(\rho_i) = \rho_i E_{mat}$, where $\rho_i \in [0, 1]$ and E_{mat} is the elastic modulus of the solid material when the thickness assumes its maximum value ($\rho_i = 1$). To overcome computational issues in case of zero-stiffness elements, we redefine the range of

each ρ_i as $[\rho_{min}, 1]$, with $\rho_{min} > 0$, which is equivalent to what presented in (1). The goal of our STO is to find the best vector $\boldsymbol{\rho} = [\rho_1 \dots \rho_N]$ that minimizes $\widehat{C}(\boldsymbol{\rho})$, given one or more constraints on the ρ_i values. In the following, as constraint, we impose a fixed value ρ^* to the mean ρ_i over the elements.

Thus, the nominal problem is:

$$\text{minimize} \quad \widehat{C}(\boldsymbol{\rho})$$

s.t.

$$\begin{cases} \text{Linear elastic problem in function of } \boldsymbol{\rho} \\ \dfrac{\sum_{i=1}^{N} \rho_i}{N} = \rho^* \\ \rho_{min} \leq \rho_i \leq 1, \qquad i = 1, \dots, N \end{cases}$$

Actually, we refer to the discretized counterpart of (2), namely:

$$C = \tilde{\boldsymbol{u}}' \, \mathbb{K} \, \tilde{\boldsymbol{u}} \tag{3}$$

with $\mathbb{K}\tilde{\boldsymbol{u}} = \boldsymbol{F}$, where $\tilde{\boldsymbol{u}}$, $\boldsymbol{F}$ and $\mathbb{K}$ are the discretized displacement vector, force vector and stiffness matrix, respectively. Symbol $'$ denotes matrix transposition.

Moreover, as for the densities ρ_i, we add the well-known linear density filter (Sigmund, 2007), considering the following filtered densities $\bar{\rho}_i$:

$$\bar{\rho}_i = \frac{\sum_{j \in N_i} h\left(\boldsymbol{y}_j\right) A_j \rho_j}{\sum_{j \in N_i} h\left(\boldsymbol{y}_j\right) A_j} \tag{4}$$

A_j and $\boldsymbol{x}_j$ are the area and the center location of element j, respectively, while $\boldsymbol{y}_j$ appearing in the formula is a transformed vector for the coordinates such that $\boldsymbol{y}_j = \boldsymbol{\Gamma}\boldsymbol{x}_j$. N_i is the neighborhood of element i, defined as:

$$N_i = \{k : \|\boldsymbol{y}_k - \boldsymbol{y}_i\| < R\}$$

and $h\left(\boldsymbol{y}_j\right) = R - \left\|\boldsymbol{y}_j - \boldsymbol{y}_i\right\|$ is a linear weight function. Matrix $\boldsymbol{\Gamma}$ allows us to consider different shapes for the neighborhood of the elements. In this way, the elastic modulus E_i is redefined as:

$$E_i(\bar{\rho}_i) = \bar{\rho}_i E_{mat} \tag{5}$$

Thus, the addressed problem is stated as follows:

$$\text{minimize} \quad C(\bar{\boldsymbol{\rho}}) \tag{6}$$

s.t.

$$\begin{cases} \text{Discretized linear elastic problem in function of } \bar{\boldsymbol{\rho}} \\ \bar{\rho}_i = \dfrac{\displaystyle\sum_{j \in N_i} h\left(\boldsymbol{\Gamma} \boldsymbol{x}_j\right) A_j \rho_j}{\displaystyle\sum_{j \in N_i} h\left(\boldsymbol{\Gamma} \boldsymbol{x}_j\right) A_j} \\ \dfrac{\sum_{i=1}^{N} \rho_i}{N} = \rho^* \\ \rho_{min} \leq \rho_i \leq 1, \qquad i = 1, \ldots, N \end{cases} \tag{7}$$

with $\bar{\boldsymbol{\rho}} = [\bar{\rho}_1 \ldots \bar{\rho}_N]'$.

3.2. Building a reduced basis via FPCA

The methodological content of this section is based on the FPCA reduction approach developed in Bianchini et al. (2015); the interested reader can refer to such a reference for further details. However, as mentioned, the objective of Bianchini et al. (2015) was to investigate the variability of a certain output quantity of interest given that some mechanical parameters are random. Here, on the contrary, the optimization problem does not include any randomness/variability, since we are looking for the (deterministic) configuration of parameters that leads to the optimal output. This difference does not prevent us from exploiting the FPCA reduction approach as in Bianchini et al. (2015), even though some precautions are needed (as discussed in Sect. 3.4).

3.2.1. FPCA for FEA

Let $\mathcal{U}(\Theta) = \{\boldsymbol{u}(\boldsymbol{x}, \boldsymbol{\rho}), \boldsymbol{\rho} \in \Theta\} \in L^2(\Omega)$ be the solutions space of the structural problem, with $\Theta = [\rho_{min}, 1]^N$. The goal of the FPCA is to describe $\mathcal{U}(\Theta)$ through an optimal orthonormal basis.

For this purpose, we need M realizations of the solution, obtained with as many values $\boldsymbol{\rho}_m$ $(m = 1, \ldots, M)$ of the parameter vector $\boldsymbol{\rho}$; of course, the bigger M is, the more accurate the procedure will be.

By assuming that M is large enough, the subspace spanned by the solutions

$$\{\boldsymbol{u}(\boldsymbol{x}, \boldsymbol{\rho}_m), m = 1, \ldots, M\}$$

approximates $\mathcal{U}(\Theta)$. Thus, by applying FPCA to these solutions, we may estimate the K orthonormal basis functions that optimally approximate $\mathcal{U}(\Theta)$, where K is a fixed integer value with $1 \leqslant K \leqslant M$.

Indeed, FPCA is a method to build an approximation of the set of solutions. Let us denote by $v_m(\boldsymbol{x})$ the solution $\boldsymbol{u}(\boldsymbol{x}, \boldsymbol{\rho}_m)$ and by $\hat{v}_m(\boldsymbol{x})$ the corresponding approximate solution.

The approximation takes the following form:

$$\hat{v}_m(\boldsymbol{x}) = \sum_{k=1}^{K} f_{mk}\ \xi_k(\boldsymbol{x})$$

where $\xi_k(\boldsymbol{x})$, $k = 1, \ldots, K$ are the orthonormal *principal functions* and f_{mk} the *principal component scores* corresponding to the m-th solution, which are defined as:

$$f_{mk} = \int_{\Omega} v_m(\boldsymbol{s})\ \xi_k(\boldsymbol{s})\ d\boldsymbol{s} \qquad k = 1, \ldots, K$$

The data-driven basis we are considering collects the principal functions. This basis is optimal, as the K functions $\{\xi_k(\boldsymbol{x}), k = 1, \ldots, K\}$ achieve the minimum of the following error measure χ, given the M observed functions $\{v_m(\boldsymbol{x}), m = 1, \ldots, M\}$:

$$\chi = \sum_{m=1}^{M} \|v_m - \hat{v}_m\|_{L^2}^2 = \sum_{m=1}^{M} \int_{\Omega} \left(v_m(\boldsymbol{s}) - \hat{v}_m(\boldsymbol{s})\right)^2 d\boldsymbol{s}$$

In other words, the basis minimizes the sum of the L^2 reconstruction errors over the M data.

From an operative viewpoint, the elements of the basis solve a particular eigenvalue problem which involves the covariance operator. Let us consider M functions $\{v_m(\boldsymbol{x}), m = 1, \ldots, M\}$ with a null cross-sectional mean, i.e.,

$$\frac{1}{M} \sum_{m=1}^{M} v_m(\boldsymbol{x}) = 0$$

Then, the associated (empirical) covariance function is defined as:

$$\mathbb{V}(\boldsymbol{s}, \boldsymbol{t}) = \frac{1}{M} \sum_{m=1}^{M} v_m(\boldsymbol{s}) v_m(\boldsymbol{t})$$

and the corresponding *covariance operator* as:

$$\mathbf{V}\xi : \xi(\cdot) \mapsto \int_{\Omega} \mathbb{V}(\cdot, \boldsymbol{t}) \xi(\boldsymbol{t}) d\boldsymbol{t}$$

Hence, each principal component turns out to solve the following eigenproblem:

$$\mathbf{V}\xi(\boldsymbol{x}) = \gamma \xi(\boldsymbol{x}) \tag{8}$$

and the FPCA can be equivalently expressed as the eigenanalysis of the covariance operator $\mathbf{V}$. This characterization helps us in building the basis, as explained in the next section.

3.2.2. Creation of the reduced basis

We start from M solutions $\boldsymbol{u}_1(\boldsymbol{x}), \ldots, \boldsymbol{u}_M(\boldsymbol{x})$ obtained solving complete FEA problems for different values of $\boldsymbol{\rho}$, and we define the matrix

$$\mathbb{U} = [\tilde{\boldsymbol{u}}(\boldsymbol{\rho}_1) - \bar{\boldsymbol{u}}, \ldots, \tilde{\boldsymbol{u}}(\boldsymbol{\rho}_M) - \bar{\boldsymbol{u}}]'$$

where $\tilde{\boldsymbol{u}}(\boldsymbol{\rho}_m)$ is the vector containing the displacements in all of nodes of the FEA mesh (ordered as the displacements of the first node, then of the second node, and so on) and $\bar{\boldsymbol{u}}$ is the sample mean

$$\bar{\boldsymbol{u}} = \frac{1}{M} \sum_{m=1}^{M} \tilde{\boldsymbol{u}}(\boldsymbol{\rho}_m)$$

Thus, the dimension of $\mathbb{U}$ is $M \times 2L$, where L is the number of elements of the mesh.

We have to find out the orthonormal basis based on the functional principal components of matrix $\mathbb{U}$. We suggest to use the method of snapshots (Sirovich, 1987; Volkwein, 2011) to determine the basis: if $2L > M$, which is certainly our case, the basis of rank K is determined as follows:

- define $\mathbb{Y} = (\mathbb{U}\mathbb{W}^{1/2})'$ with

$$\mathbb{W} = [w_{b_1 b_2}] \left[\int \phi_{b_1}(\boldsymbol{x}) \phi_{b_2}(\boldsymbol{x}) d\boldsymbol{x} \right]$$

  where $\phi_k(\cdot)$ are the finite element functions;

- solve the eigenvalue problem

$$\mathbb{Y}'\mathbb{Y}\boldsymbol{v}_k = \lambda_k \boldsymbol{v}_k \qquad k = 1, \ldots, K$$

  where λ_k are in descending order;

- set

$$\boldsymbol{\xi}_k = \frac{1}{\sqrt{\lambda_k}} \mathbb{U}'\boldsymbol{v}_k \qquad k = 1, \ldots, K.$$

The projection into the reduced space of dimension K can be done using the following matrix:

$$\mathbb{U}_{rb} = [\boldsymbol{\xi}_1, \ldots, \boldsymbol{\xi}_K].$$

Finally, we have to choose the value of K. We adopt a method based on the maximum eigenvalue λ_{max}, i.e., we retain all of the eigenfunctions corresponding to an eigenvalue λ_k such that $\lambda_k > \Lambda\lambda_{max}$, where Λ typically assumes small values, e.g., 10^{-4} (Dulong et al., 2007).

3.2.3. Reduced FEA problem

We employ the reduced basis because, at each iteration g of the optimization method (e.g., the SA adopted in this work), we solve a *reduced* problem, which is much less computationally demanding as the solution is obtained in the subspace spanned by the principal components.

The complete FEA problem corresponding to the linear elastic problem requires to solve

$$\mathbb{K}_g \tilde{\boldsymbol{u}}_g = \boldsymbol{F} \tag{9}$$

where $\mathbb{K}_g$ is the stiffness matrix for realization $\boldsymbol{\rho}_g$.

On the contrary, the reduced problem is obtained by projecting the problem into the subspace spanned by the K principal components:

$$\mathbb{U}'_{rb}\mathbb{K}_g \tilde{\boldsymbol{u}}_{red,g} = \mathbb{U}'_{rb}\boldsymbol{F}, \tag{10}$$

with $\tilde{\boldsymbol{u}}_{red,g} = \bar{\boldsymbol{u}}_g + \mathbb{U}_{rb}\mathbb{U}'_{rb}\boldsymbol{u}_g = \bar{\boldsymbol{u}} + \mathbb{U}_{rb}\boldsymbol{a}_g$ and $\boldsymbol{a}_g = \mathbb{U}'_{rb}\boldsymbol{u}_g \in \mathbb{R}^k$. Thus projection (10) becomes:

$$\mathbb{U}'_{rb}\mathbb{K}_g\mathbb{U}_{rb}\boldsymbol{a}_g + \mathbb{U}'_{rb}\mathbb{K}_g\bar{\boldsymbol{u}}_g = \mathbb{U}'_{rb}\boldsymbol{F}$$

Summing up, for each iteration/realization g, the reduced problem turns out to be the following:

$$\begin{cases} \mathbb{K}_{rb}\boldsymbol{a}_g = \boldsymbol{F}_{rb} \\ \tilde{\boldsymbol{u}}_{red,g} = \mathbb{U}_{rb}\boldsymbol{a}_g \\ \tilde{\boldsymbol{u}}_g = \bar{\boldsymbol{u}}_g + \tilde{\boldsymbol{u}}_{red,g} \end{cases} \tag{11}$$

with:

- $\mathbb{K}_{rb} = \mathbb{U}'_{rb}\mathbb{K}_g\mathbb{U}_{rb}$;
- $\boldsymbol{F}_{rb} = \mathbb{U}'_{rb}\boldsymbol{F} - \mathbb{U}'_{rb}\mathbb{K}_g\bar{\boldsymbol{u}}_g = \mathbb{U}'_{rb}\left(\boldsymbol{F} - \mathbb{K}_g\bar{\boldsymbol{u}}_g\right)$.

Obviously, the solution $\tilde{\boldsymbol{u}}_g$ of (11) is computationally cheaper than the solution obtained when solving a complete FEA problem, but it is only an approximation. To monitor the approximation error, we compute at each iteration g the residual $\tilde{\boldsymbol{e}}_{red,g} = \mathbb{K}_g\tilde{\boldsymbol{u}}_{red,g} - \boldsymbol{F}$ and consider its quadratic norm

$$err_g = \|\boldsymbol{e}_{red,g}\|^2_{L^2} = \tilde{\boldsymbol{e}}'_{red,g}\mathbb{W}\tilde{\boldsymbol{e}}_{red,g}$$

as an estimate for the error.

We check whether $err_g < tol$, where tol is a tolerance value defined by the user. If the condition is satisfied, we keep the reduced solution for iteration g and go ahead with the next iteration $g+1$. Conversely, if the condition is not satisfied, we discard the reduced solution and solve the full problem. The complete solution of the full problem is kept for iteration

g, and it is also used as a further realization to update the basis. The newly updated basis replaces the previous one for all of the following iterations of the algorithm, until a new update is required.

Anyway, the construction of the reduced FPCA basis requires several FEA solutions; thus, at the first M^* iterations, the complete FEA problem is directly solved.

3.3. Simulated annealing algorithm

We employ the classical framework of the SA iterative algorithm, in which the optimal solution S^* is refined iteration by iteration (Henderson et al., 2003). Below, we briefly recall the framework and we detail the main points of our implementation.

In general, at each iteration g of the algorithm, a new solution S_g is computed based on a given value $\boldsymbol{\rho}_g$. If the newly provided solution S_g has a better value of the objective function than the current optimal solution S^*, new solution S_g replaces the current S^*, and the value $\boldsymbol{\rho}_{g+1}$ for the next iteration is computed based on the current one $\boldsymbol{\rho}_g$. Otherwise, the provided solution S_g can be accepted with a probability π_g. If accepted, once again S_g replaces the current S^*, and the value $\boldsymbol{\rho}_{g+1}$ is computed based on $\boldsymbol{\rho}_g$. If not accepted, the solution S_g is not considered and the value $\boldsymbol{\rho}_{g+1}$ is computed based on that of the current optimal solution $\boldsymbol{\rho}^*$. The solution S^* at the end of the iterations is the optimal solution provided by the SA.

In our work, each solution S_g refers to problem (7), once a value $\boldsymbol{\rho}_g$ is fixed. To complete the description of the algorithm, we must provide the approach to compute the next value $\boldsymbol{\rho}_{g+1}$ while respecting the mean ρ^*, the rule to compute probability π_g, the initialization of the algorithm, and the termination criteria.

As for the next value $\boldsymbol{\rho}_{g+1}$, it is built by first adding a discrete Gaussian random field with null mean to the current density field. Then, values outside of the range $[\rho_{min}, 1]$ are replaced with the closest value in the range, and the resulting field is normalized to respect that the mean value is ρ^*. The Gaussian field is generated at each iteration, while its covariance matrix is updated every g_{gauss} iterations, to start from highly variable fields to highly correlated ones.

Indeed, each element of the covariance matrix is given by $\sigma e^{d\left(\boldsymbol{y}_i, \boldsymbol{y}_j\right)\phi_g}$, where $d\left(\boldsymbol{y}_i, \boldsymbol{y}_j\right)$ is the Euclidean distance between the transformed coordinates $\boldsymbol{y}_i$ and $\boldsymbol{y}_j$ of elements i and j, respectively, and ϕ_g is as follows:

$$\phi_g = \phi_{final} - \left(\phi_{final} - \phi_{init}\right) e^{-g_{start}/\mathcal{T}_{gauss}}$$

where g_{start} represents the first value of g within the group of g_{gauss} iterations, and $\phi_{final} < \phi_{init}$.

Concerning π_g, it is based on a *cooling schedule*, i.e., a strictly monotonic decreasing *temperature* function $T(g)$. In our case, we consider the following form:

$$T(g) = T_{max} e^{-g/\mathcal{T}_{sa}}$$

Then, π_g is given by:

$$\pi_g = e^{-\frac{C_g - C^*}{T(g)}}$$

where C_g and C^* refer to the objective function (compliance) values for S_g and S^*, respectively. To evaluate whether to accept a worst solution S_g with $C_g > C^*$, a random number η_g uniformly distributed between 0 and 1 is generated; if $\eta_g < \pi_g$, then the solution is accepted. According to the SA framework, accepting a worst solution becomes less likely while g increases, as $T(g)$ monotonically decreases with g.

Finally, the algorithm is initialized considering a vector $\boldsymbol{\rho}_1$ in which all elements are equal to ρ^*, while it is terminated after a maximum number G of iterations or when the solution *freezes*. The latter, according to the SA framework, occurs when the current optimal solution S^* is not updated in the last g_f iterations and $T(g)$ is below a given value T_f.

The adopted values of all parameters are reported in the computational analyses (Sect. 5.1).

3.4. Making the basis adaptive

The two ingredients introduced in Sect. 3.2 and 3.3 are combined to build an algorithm that efficiently solves the STO. Thus, the goal of the reduced basis is to solve an optimization problem whose characteristics vary along with the iterations g of the optimization.

In particular, the value of $\boldsymbol{\rho}_g$ changes at each iteration, and after several iterations the analyzed FEA problem can be strongly different from the previous ones. As a consequence, we need a basis that *follows* the changes happening along with the iterations.

For this reason, when an update of the basis is required (because $err_g \geq tol$), the new basis is built considering only the last solutions obtained solving a complete FEA problem. In particular, we consider the last M^* solutions, where M^* coincides with the number of the initial complete solutions (end of Sect. 3.2.3).

In this way, we get rid of the *old* solutions that are likely to be very different from the current one, and thus not useful to describe the space $\mathcal{U}(\Theta)$ in the neighborhood of the current point. In the absence of such riding, the dimension of the reduced problem could be uselessly higher, because of including additional variability related to conditions very far from those currently under investigation. Moreover, including the useless variability, the error related to the reduced problem could increase.

4. Test case

We validate the proposed approach dealing with one of the classical problems encountered in STO, i.e., the compliance minimization for a variable thickness cantilever sheet.

The cantilever consists of a rectangular domain Ω (dimension $b \times h$) with Dirichlet boundary conditions on one of the sides. Moreover, as load, we either consider a constant body force $\boldsymbol{f}_d$ or a concentrated force $\boldsymbol{f}_c$ applied in the middle of the side opposite to the

one with Dirichlet boundary conditions. The domain, together with the Dirichlet conditions and the two alternative loads, is sketched below.

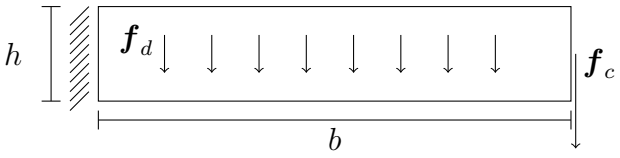

The setting for the tested cases is: $\Omega = (0, 200) \times (0, 40)$; either $\boldsymbol{f}_d = (0, -0.1)$ or $\boldsymbol{f}_c = (0, -10)$; Poisson's ratio $\nu = 0.3$; $E_{mat} = 2000$; $\rho_{min} = 0.05$.

We adopt a standard FEA discretization to solve the problem, based on triangular bi-linear approximations into a standard principle of virtual work approximation (Zhu et al., 2005; Hughes, 2012), where n is the number of intervals between nodes per each side of the domain.

As for ρ_i, we discretize the domain into N rectangular elements, each one involving two triangular regions of the mesh; thus, $L = 2N$ and $n = \sqrt{N}$.

Finally, as for the density filter, we adopt $R = 2$ the following diagonal matrix Γ:

$$\Gamma = \begin{bmatrix} \frac{n}{b} & 0 \\ 0 & \frac{n}{h} \end{bmatrix}$$

so as to have an elliptic neighbor region for (4), whose semiaxes are proportional to the size of the elements in that direction.

5. Computational analyses

We first consider one mechanical condition to evaluate the impact of the FPCA parameters (Sect. 5.1). Then, fixing these parameters to a suitable value, we investigate several mechanical conditions to analyze the STO outcomes (Sect. 5.2). Finally, in the same section, we compare our outcomes with a literature benchmark.

All tests have been run on a Server with processor X86-64 AMD Opteron 6328 and 64GB of dedicated RAM.

5.1. Impact of FPCA parameters

These analyses are conducted under concentrated force with $\rho^* = 0.5$. The analyses refer to the impact of n, *tol*, Λ and M. In particular, 3 levels for n (50, 70 and 90), 3 levels for *tol* (5%, 7.5% and 10%), 2 levels for Λ (10^{-7} and 10^{-4}) and 2 levels for M^* (30 and 50) are considered.

The other SA parameters are fixed as follows: $G = 2000$; $T_{max} = 0.0004$; $\mathcal{T}_{sa} = 1000$; $T_f = 10$; $g_f = 2000$ (the latter two values are set to prevent early freezing). Finally,

the additional parameters for the Gaussian field are as follows: $g_{gauss} = 50$; $\sigma = 0.0005$; $\phi_{init} = 250/n$; $\phi_{final} = 0.025/n$; $\mathcal{T}_{gauss} = 500$.

All tests are reported in Table 1 together with the main outcomes, i.e., the objective function C, the mean computational time to run a complete FEA, the number of rejections of the reduced FEA solution (because $err_g \geq tol$), the mean computational time to run a reduced FEA, the mean time to create a new basis, and the maximum number K of vectors in the basis along with the iterations.

Results clearly show that the computational time required by the reduced FEA is one order of magnitude lower than the time required by the complete FEA, and that the difference grows with n. Moreover, the time to compute the basis is about one-fourth of the time required by the complete FEA.

Details are reported in Figure 1. Plots show that the time required by the complete FEA strongly increases with n, while on the contrary the increasing of the time required by the reduced FEA is negligible; thus, this dramatically increases the difference between the times while n increases. Also the time for creating the basis increases, but again the difference between the time for the complete FEA and the time for computing the basis increases with n. Results are retained while varying the other parameters, e.g., parameter tol as in the three plots of Figure 1.

Moreover, it is worth noting that the other outcomes are about the same while varying n; in particular, the reached objective function and the number of rejections do not seem to be affected by n.

As expected, the number of rejections varies along with tol, while it only marginally depends on other parameters (see Figure 2a as example) showing only a small reduction from $M^* = 30$ to $M^* = 50$. Also the objective function C varies with tol, as expected, as higher tol values increase the error associated with the FEA solutions, thus resulting in an error associated with the objective function C.

Anyway, the variation of the objective function C is limited and below an approximation universally accepted for FEA methods. In particular, by comparing the solutions in Table 1 with the corresponding ones without reduced basis (i.e., when $tol = 0\%$ and the reduced solution is never exploited), errors are below the 3% in the majority of cases.

A trade-off is required; in our case we consider $tol = 7.5\%$ as the optimal choice because it gives limited variations of objective functions C with respect to $tol = 0\%$, and because the largest reduction in the number of rejections is observed between $tol = 5\%$ and $tol = 7.5\%$.

As for the impact of Λ, we observe that with $\Lambda = 10^{-7}$ the maximum number K of vectors in the basis along with the iterations is always equal to $M - 1$, meaning that all eigenvectors are always included. On the contrary, with $\Lambda = 10^{-4}$, a lower number of vectors

Input parameters				**Outcomes**					
n	tol	Λ	M^*	Objective function C	Mean time complete FEA [s]	Number of rejections	Mean time reduced FEA [s]	Mean time create basis [s]	Max K iter.
50	0.0%	– – –	–	14.400	0.08512	– –	– – –	– – –	–
50	5.0%	10^{-7}	30	14.444	0.08321	776	0.00531	0.02354	29
50	7.5%	10^{-7}	30	14.747	0.09130	275	0.00491	0.02263	29
50	10.0%	10^{-7}	30	14.862	0.08900	147	0.00415	0.02167	29
50	5.0%	10^{-4}	30	14.431	0.11150	1054	0.00199	0.01781	21
50	7.5%	10^{-4}	30	14.651	0.11062	338	0.00148	0.01599	17
50	10.0%	10^{-4}	30	14.891	0.11201	157	0.00117	0.01602	14
50	5.0%	10^{-7}	50	14.457	0.09603	778	0.00751	0.05052	49
50	7.5%	10^{-7}	50	14.697	0.10351	299	0.00716	0.04851	49
50	10.0%	10^{-7}	50	14.582	0.10722	174	0.00645	0.04515	49
50	5.0%	10^{-4}	50	14.408	0.10171	1114	0.00219	0.03012	23
50	7.5%	10^{-4}	50	14.578	0.11304	472	0.00208	0.02881	22
50	10.0%	10^{-4}	50	14.887	0.10381	222	0.00115	0.02745	8
70	0.0%	– – –	–	14.472	0.21073	– –	– – –	– – –	–
70	5.0%	10^{-7}	30	14.640	0.20505	791	0.01255	0.05190	29
70	7.5%	10^{-7}	30	14.849	0.23546	265	0.01312	0.05478	29
70	10.0%	10^{-7}	30	15.007	0.22744	163	0.01239	0.05317	29
70	5.0%	10^{-4}	30	14.551	0.20557	1084	0.00412	0.03451	23
70	7.5%	10^{-4}	30	14.832	0.20600	299	0.00271	0.02948	12
70	10.0%	10^{-4}	30	18.168	0.20656	80	0.00234	0.02889	5
70	5.0%	10^{-7}	50	14.535	0.21838	876	0.01693	0.10878	49
70	7.5%	10^{-7}	50	14.634	0.24926	310	0.01854	0.12620	49
70	10.0%	10^{-7}	50	14.847	0.24915	172	0.01435	0.09257	49
70	5.0%	10^{-4}	50	14.557	0.20208	1143	0.00403	0.05726	25
70	7.5%	10^{-4}	50	15.025	0.19835	387	0.00258	0.05104	11
70	10.0%	10^{-4}	50	15.166	0.20014	258	0.00215	0.04994	6
90	0.0%	– – –	–	14.495	0.35333	– –	– – –	– – –	–
90	5.0%	10^{-4}	30	14.682	0.36901	973	0.00735	0.06166	21
90	7.5%	10^{-4}	30	16.050	0.36560	212	0.00434	0.05751	5
90	10.0%	10^{-4}	30	15.707	0.36508	117	0.00414	0.05663	5

Table 1: Tested cases for concentrated force with $\rho^* = 0.5$.

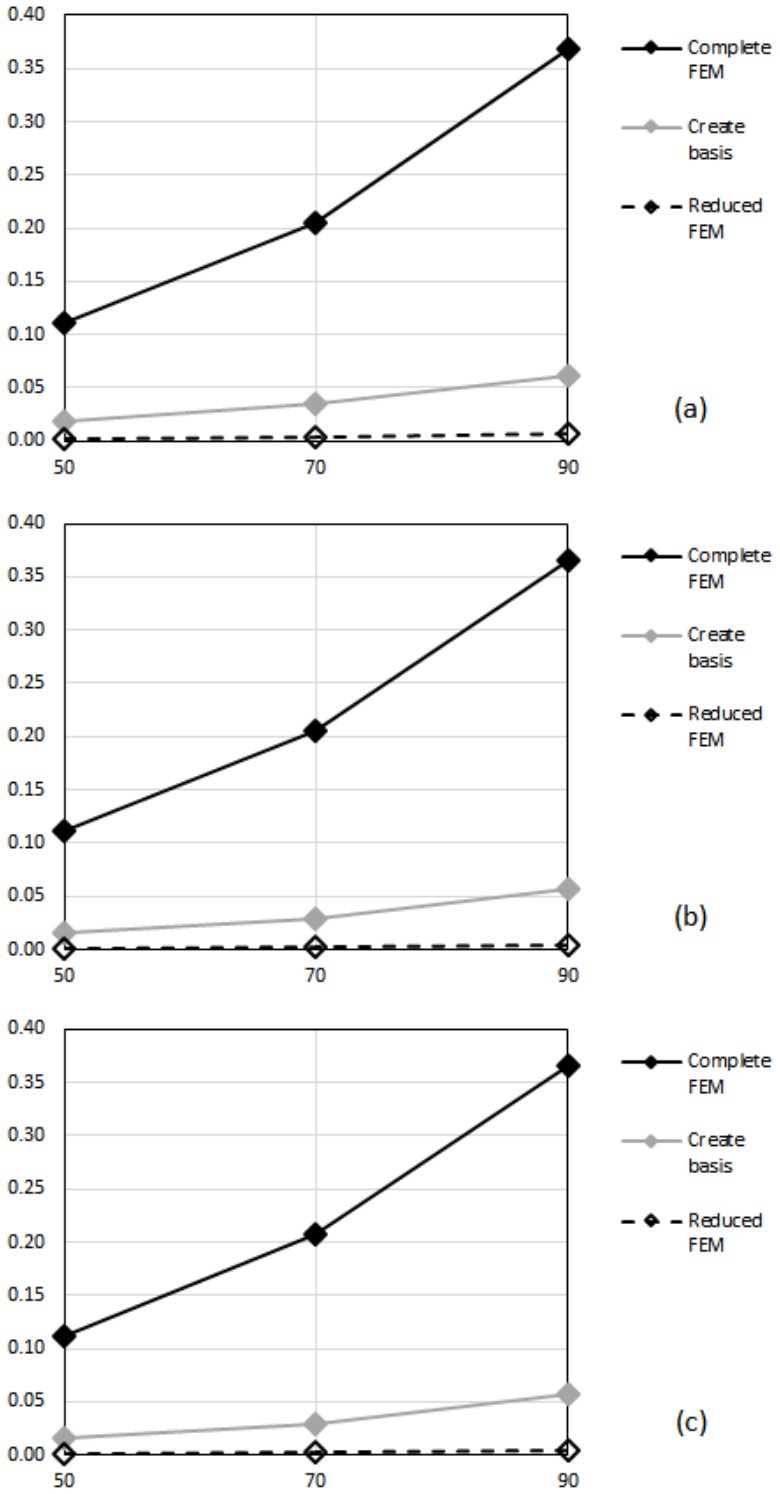

Figure 1: Mean time to run a complete FEA, to run a reduced FEA, and to create the basis as a function of n for $tol = 5\%$ (a), $tol = 7.5\%$ (b) and $tol = 10\%$ (c); other parameters are $\Lambda = 10^{-4}$ and $M^* = 30$.

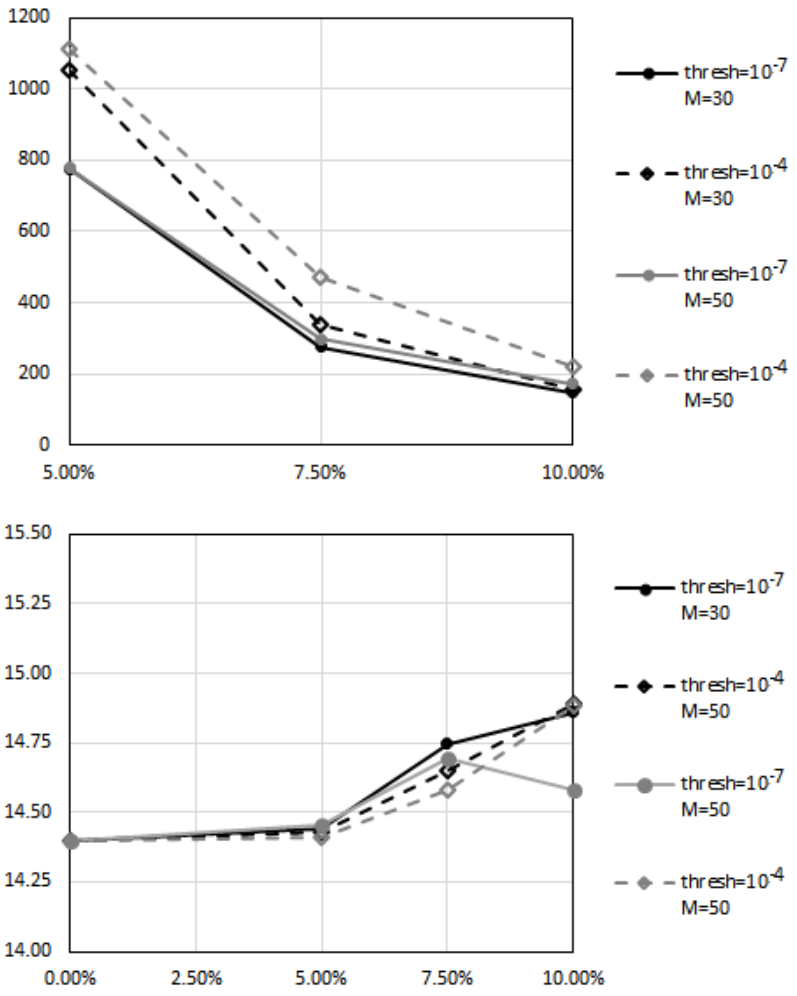

Figure 2: Number of rejected reduced FEA solutions (a) and objective function C (b) as a function of tol, for $\Lambda = 10^{-7}$ or $\Lambda = 10^{-4}$, and $M^* = 30$ or $M^* = 50$; $n = 50$ in all cases.

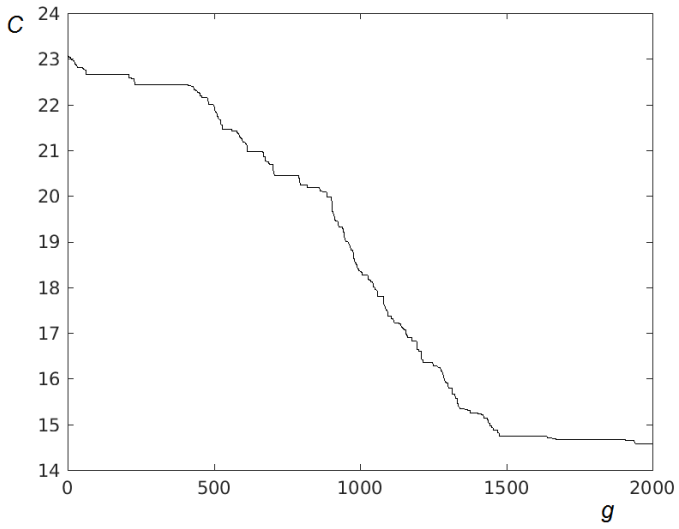

Figure 3: Objective function along with the iterations for concentrated force, $\rho^* = 0.5$, $tol = 7.5\%$, $\Lambda = 10^{-4}$ and $M^* = 50$.

is included. This happens with both $M^* = 30$ and $M^* = 50$. As all other outcomes do not change with Λ, we consider the simplest case in the following analyses, i.e., $\Lambda = 10^{-4}$ and $M^* = 50$.

5.1.1. Convergence of the simulated annealing

Even though the SA employed in the STO is not the core of our work, we verify the convergence of the algorithm in order to rely on the obtained results.

Figure 3 shows the objective function along with the 2000 iterations for the same case of concentrated force with $\rho^* = 0.5$, in which the above selected parameters are taken (i.e., $tol = 7.5\%$, $\Lambda = 10^{-4}$ and $M^* = 50$).

The trend shows the convergence of the algorithm, with a plateau in the objective functions after a certain number of iterations. Thus, with the selected parameters for the SA, the algorithm is able to converge. We remark that there we did not observe freezing before the end of the programmed iterations because of the set parameters.

Similar trends with a plateau sufficiently before $g = 2000$ are obtained in all other cases of Table 1.

5.2. Mechanical outcomes

In this section we consider several mechanical conditions to further analyze the behavior of the approach and provide solutions that can be compared with literature benchmarks. Analyses are conducted at three different levels of ρ^* (i.e., $\rho^* = 0.25$, $\rho^* = 0.5$ and $\rho^* = 0.75$), and both under concentrated and distributed force, whose values are reported in Sect. 4.

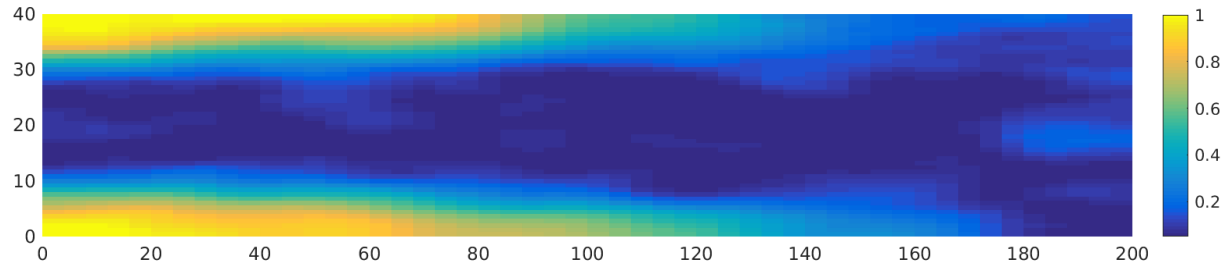

(a)

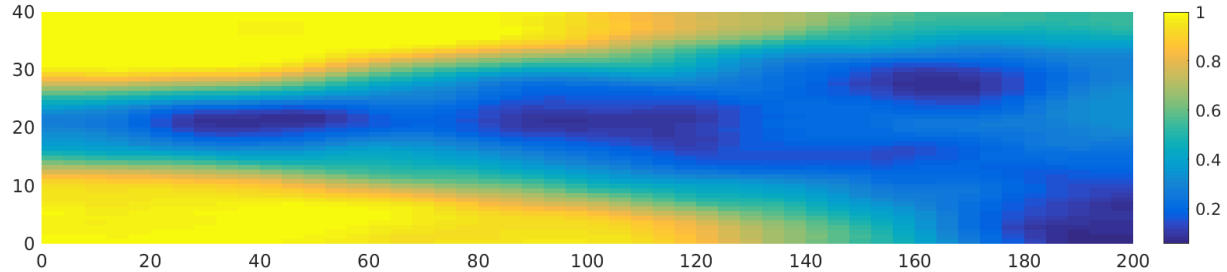

(b)

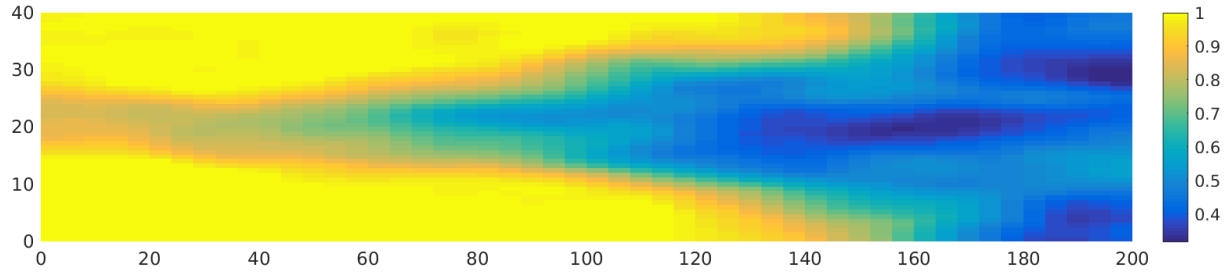

(c)

Figure 4: Map of optimal ρ as function of ρ^* in the case of concentrated force: $\rho^* = 0.25$ (a); $\rho^* = 0.5$ (b); $\rho^* = 0.75$ (c).

As for the other parameters, we consider a discretization with $n = 50$, which is enough for the considered problem, and we set $\Lambda = 10^{-4}$ and $M^* = 30$, which represent the optimal trade-off from the results presented above. Finally, all other parameters assume the same value as in Sect. 5.1.

Detailed outcomes for all tested cases are reported in Table 2, while the density maps at the optimum are provided in Figures 4 and 5. Moreover, the objective function as a function of ρ^* is reported in Fig. 6 for both the concentrated and the distributed force.

The obtained maps are coherent and reflect what we expected, based on both the structure of the addressed problem itself and the available literature.

Input parameters			**Outcomes**						**No reduced**
Force	ρ^*	tol	Objective function C	Mean time [s] compl FEA	Number rejections	Mean time [s] reduc FEA	Mean time [s] create basis	Max K	Objective function C
conc	25%	25.0%	24.045	0.08947	695	0.00290	0.02864	31	23.357
conc	50%	7.5%	14.578	0.11304	472	0.00208	0.02881	22	14.400
conc	75%	2.0%	12.196	0.10128	868	0.00119	0.02547	9	12.161
dist	25%	4000%	20953.04	0.08721	930	0.00211	0.02617	28	20703.83
dist	50%	1000%	13122.20	0.11020	910	0.00146	0.02741	18	12990.91
dist	75%	300%	11714.37	0.10574	1004	0.00112	0.02604	8	11630.48

Table 2: Summary of tested cases while varying ρ^* and the concentrated/distributed force.

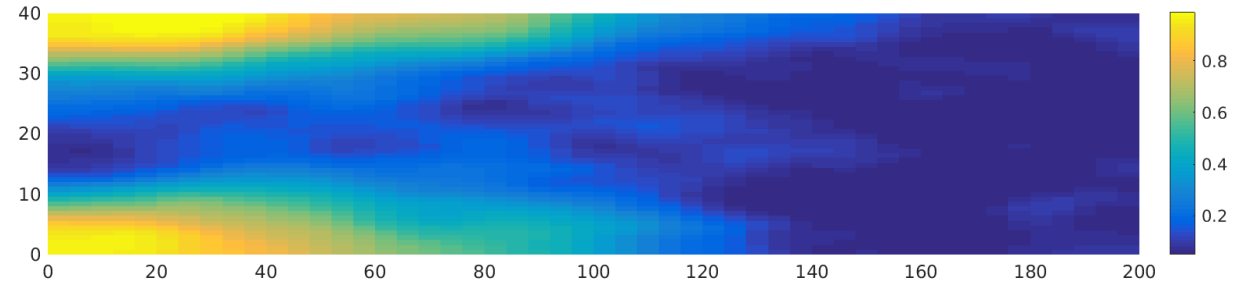

(a)

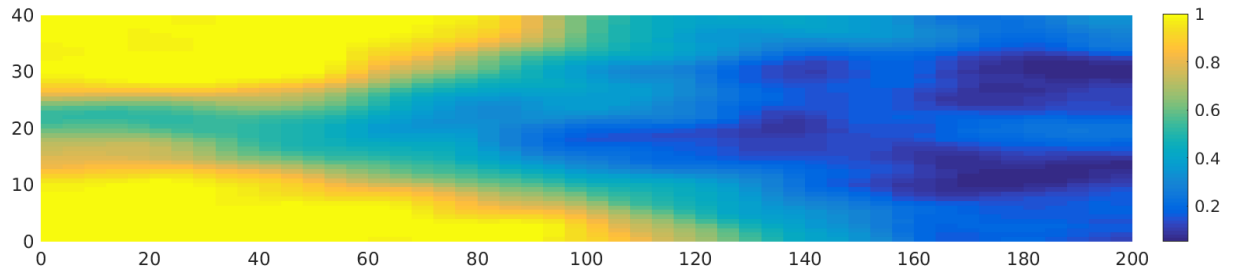

(b)

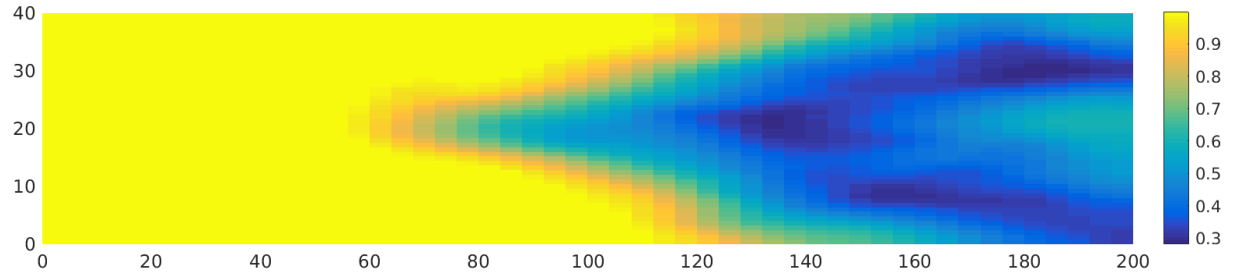

(c)

Figure 5: Map of optimal ρ as function of ρ^* in the case of distributed force: $\rho^* = 0.25$ (a); $\rho^* = 0.5$ (b); $\rho^* = 0.75$ (c).

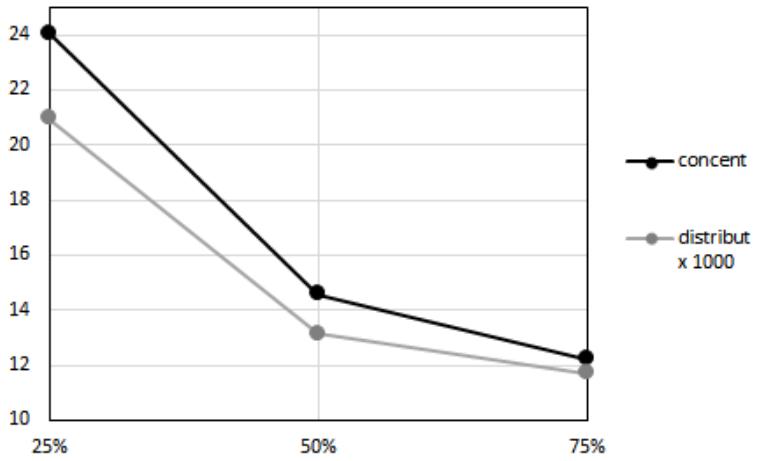

Figure 6: Objective function as a function of ρ^* under both concentrated and distributed force.

A more detailed comparison is reported below at the end of the section. However, before the comparison with the literature, let us analyze once again the obtained solutions with respect to those obtained without reduced basis (i.e., imposing $tol = 0\%$). First of all, the high reduction of the computational time between reduced and complete FEA is confirmed. Moreover, as shown in Table 2, very close values of objective function C are found when exploiting or not exploiting the reduced basis. This is also confirmed while comparing the maps in Figures 4 and 5 with the corresponding ones obtained without reduced basis (not reported in the paper). The similar maps, together with the close value of the objective function, further confirms the goodness of the optimal solution.

Finally, we remark that plots similar to Figure 3 are obtained in all cases, assessing the converge of the SA algorithm.

It may appear strange that these good solutions are found with high values of tol. Anyway, the discrepancy between a high value of tol and a satisfying approximation of the solutions is due to the fact that tol takes into account the reconstruction error of the external force $\boldsymbol{f}$, while our interest is on the solution $\boldsymbol{u}$, which gives the objective function. Therefore, it may happen that the solution $\boldsymbol{u}$ does not vary too much while changing $\boldsymbol{f}$, thus leading to a possibly large reconstruction error on $\boldsymbol{f}$ but at the same time to a good approximation of the objective function.

As benchmark for comparing our outcomes, we consider the solutions presented in Bendsøe & Sigmund (2013). Our solutions are coherent with those of the benchmark, being coincident from a qualitative point of view. In particular, both in our outcomes and in Bendsøe & Sigmund (2013), optimized solutions are obtained by increasing the density near the fixed and the external sides of the cantilever. We also observe considerable areas with intermediate density, especially for higher values of ρ^*.

6. Discussions and conclusion

In this work, we apply FPCA to STO in order to reduce the computational times associated with the many solutions of the FEA problem, due to the iterative algorithms applied to find the optimal solution.

The outcomes from the application to one of the classical problems encountered in STO, i.e., the compliance minimization for a variable thickness cantilever sheet, are highly promising. Indeed, with a reasonable set of parameters, we have been able to provide good solutions and to reduce of at least one order of magnitude the time to solve the FEA problem in a high number of iterations.

Moreover, let us remind that optimized solutions like those shown in Figures 4 and 5 can be easily produced with the new emerging manufacturing processes, e.g., the 3D printing. Thus, STO is a necessary step of the design process to fully exploit the potentialities of such new technologies, in order to build lightweight optimized components. In this light, proposing new approaches and methodologies to reduce the computational times of STO, as the one developed in this paper, is fundamental to support the new design processes and to exploit the new technologies.

Our future work will extend the approach to the size and the shape optimization, in which the solution must follow predefined configurations. As for example, we will introduce reinforced edges or reinforced linear structures in the domain Ω, and we will optimize the solution with respect to the layout of these structures. Moreover, we will also apply our reduced basis approach to STO in the presence of gradient-based algorithms; indeed, we will investigate how to numerically evaluate the gradient of the objective function in the reduced space, allowing for a supplemental time reduction.

References

Ambrosio, L., & Buttazzo, G. (1993). An optimal design problem with perimeter penalization. *Calculus of Variations and Partial Differential Equations*, *1*, 55–69.

Bendsøe, M., & Sigmund, O. (2013). *Topology optimization: theory, methods, and applications*. (2nd ed.). Springer.

Bendsøe, M. P. (1989). Optimal shape design as a material distribution problem. *Structural optimization*, *1*, 193–202.

Bendsøe, M. P., & Kikuchi, N. (1988). Generating optimal topologies in structural design using a homogenization method. *Computer methods in applied mechanics and engineering*, *71*, 197–224.

Bianchini, I., Argiento, R., Auricchio, F., & Lanzarone, E. (2015). Efficient uncertainty quantification in stochastic finite element analysis based on functional principal components. *Computational Mechanics*, *56*, 533–549.

Borrvall, T., & Petersson, J. (2001). Large-scale topology optimization in 3D using parallel computing. *Computer methods in applied mechanics and engineering*, *190*, 6201–6229.

Bourdin, B. (2001). Filters in topology optimization. *International Journal for Numerical Methods in Engineering*, *50*, 2143–2158.

Bruns, T. E., & Tortorelli, D. A. (2001). Topology optimization of non-linear elastic structures and compliant mechanisms. *Computer Methods in Applied Mechanics and Engineering*, *190*, 3443–3459.

Chinesta, F., Keunings, R., & Leygue, A. (2013). *The proper generalized decomposition for advanced numerical simulations: a primer*. Springer Science & Business Media.

Chinesta, F., Ladeveze, P., & Cueto, E. (2011). A short review on model order reduction based on proper generalized decomposition. *Archives of Computational Methods in Engineering*, *18*, 395–404.

Dulong, J.-L., Druesne, F., & Villon, P. (2007). A model reduction approach for real-time part deformation with nonlinear mechanical behavior. *International Journal on Interactive Design and Manufacturing (IJIDeM)*, *1*, 229–238.

Florentin, E., & Díez, P. (2012). Adaptive reduced basis strategy based on goal oriented error assessment for stochastic problems. *Computer Methods in Applied Mechanics and Engineering*, *225*, 116–127.

Ghanem, R. G., & Spanos, P. D. (1991). *Stochastic finite elements: a spectral approach* volume 387974563. Springer.

Haber, R., Jog, C., & Bendsøe, M. P. (1996). A new approach to variable-topology shape design using a constraint on perimeter. *Structural Optimization*, *11*, 1–12.

Hassani, B., & Hinton, E. (2012). *Homogenization and structural topology optimization: Theory, Practice and Software*. Springer Science & Business Media.

Henderson, D., Jacobson, S. H., & Johnson, A. W. (2003). The theory and practice of simulated annealing. In *Handbook of metaheuristics* (pp. 287–319). Springer.

Horváth, L., & Kokoszka, P. (2012). *Inference for functional data with applications* volume 200. Springer.

Huang, X., & Xie, Y.-M. (2010). A further review of ESO type methods for topology optimization. *Structural and Multidisciplinary Optimization*, *41*, 671–683.

Hughes, T. J. (2012). *The finite element method: linear static and dynamic finite element analysis*. Courier Corporation.

Johnson, R. A., & Wichern, D. W. (1992). *Applied multivariate statistical analysis* volume 4. Prentice hall Englewood Cliffs, NJ.

Kerschen, G., Golinval, J.-c., Vakakis, A. F., & Bergman, L. A. (2005). The method of proper orthogonal decomposition for dynamical characterization and order reduction of mechanical systems: an overview. *Nonlinear dynamics*, *41*, 147–169.

Liorni, I., Parazzini, M., Fiocchi, S., Guadagnin, V., & Ravazzani, P. (2014). Polynomial chaos decomposition applied to stochastic dosimetry: study of the influence of the magnetic field orientation on the pregnant woman exposure at 50 Hz. In *Engineering in Medicine and Biology Society (EMBC), 2014 36th Annual International Conference of the IEEE* (pp. 342–344). IEEE.

Nouy, A. (2010). Proper generalized decompositions and separated representations for the numerical solution of high dimensional stochastic problems. *Archives of Computational Methods in Engineering*, *17*, 403–434.

Panayirci, H., & Schuëller, G.-I. (2011). On the capabilities of the polynomial chaos expansion method within SFE analysis – an overview. *Archives of computational methods in engineering*, *18*, 43–55.

Petersson, J. (1999). A finite element analysis of optimal variable thickness sheets. *SIAM journal on numerical analysis*, *36*, 1759–1778.

Ramsay, J., & Silverman, B. W. (2005). *Functional data analysis*. Wiley Online Library.

Reris, R., & Brooks, J. P. (2015). Principal component analysis and optimization: a tutorial. In *14th INFORMS Computing Society Conference* (pp. 212–225).

Ritto, T., Buezas, F., & Sampaio, R. (2012). Proper orthogonal decomposition for model reduction of

a vibroimpact system. *Journal of the Brazilian Society of Mechanical Sciences and Engineering*, *34*, 330–340.

Rozvany, G. I. N. (2009). A critical review of established methods of structural topology optimization. *Structural and Multidisciplinary Optimization*, *37*, 217–237.

Rozvany, G. I. N. (2014). *Shape and layout optimization of structural systems and optimality criteria methods* volume 325. Springer.

Rozvany, G. I. N., & Lewiński, T. (Eds.) (2014). *Topology optimization in structural and continuum mechanics*. Springer.

Sigmund, O. (1997). On the design of compliant mechanisms using topology optimization. *Journal of Structural Mechanics*, *25*, 493–524.

Sigmund, O. (2007). Morphology-based black and white filters for topology optimization. *Structural and Multidisciplinary Optimization*, *33*, 401–424.

Sigmund, O. (2011). On the usefulness of non-gradient approaches in topology optimization. *Structural and Multidisciplinary Optimization*, *43*, 589–596.

Sigmund, O., & Maute, K. (2013). Topology optimization approaches. *Structural and Multidisciplinary Optimization*, *48*, 1031–1055.

Sirovich, L. (1987). Turbulence and the dynamics of coherent structures. Part 2: symmetries and transformations. *Quarterly of Applied Mathematics*, *45*, 573–582.

Sochala, P., & Le Maître, O. (2013). Polynomial chaos expansion for subsurface flows with uncertain soil parameters. *Advances in Water Resources*, *62*, 139–154.

Umesh, K., & Ganguli, R. (2013). Material uncertainty effect on vibration control of smart composite plate using polynomial chaos expansion. *Mechanics of Advanced Materials and Structures*, *20*, 580–591.

Van Dijk, N. P., Maute, K., Langelaar, M., & Van Keulen, F. (2013). Level-set methods for structural topology optimization: a review. *Structural and Multidisciplinary Optimization*, *48*, 437–472.

Volkwein, S. (2011). Model reduction using proper orthogonal decomposition. *Lecture Notes, Institute of Mathematics and Scientific Computing, University of Graz. see http://www. uni-graz. at/imawww/volkwein/POD. pdf*, .

Xu, S., Cai, Y., & Cheng, G. (2010). Volume preserving nonlinear density filter based on heaviside functions. *Structural and Multidisciplinary Optimization*, *41*, 495–505.

Yu, H., Gillot, F., & Ichchou, M. (2012). A polynomial chaos expansion based reliability method for linear random structures. *Advances in Structural Engineering*, *15*, 2097–2112.

Zegard, T., & Paulino, G. H. (2016). Bridging topology optimization and additive manufacturing. *Structural and Multidisciplinary Optimization*, *53*, 175–192.

Zhou, M., & Rozvany, G. I. N. (1991). The COC algorithm, Part II: topological, geometrical and generalized shape optimization. *Computer Methods in Applied Mechanics and Engineering*, *89*, 309–336.

Zhu, J., Taylor, Z., & Zienkiewicz, O. (2005). *The finite element method: its basis and fundamentals*. (6th ed.). Butterworth-Heinemann.

Recent titles from the IMATI-REPORT Series:

2017

17-01: *BPX preconditioners for isogeometric analysis using analysis-suitable T-splines,* D. Cho, R. Vázquez.

17-02: *Initial-boundary value problems for nearly incompressible vector fields, and applications to the Keyfitz and Kranzer system*, A. P. Choudhury, G. Crippa, L.V. Spinolo.

17-03: *Quantitative estimates on localized finite differences for the fractional Poisson problem, and applications to regularity and spectral stability*, G. Akagi, G. Schimperna, A. Segatti, L.V. Spinolo.

17-04: *Optimality of integrability estimates for advection-diffusion equations*, S. Bianchini, M. Colombo, G. Crippa, L.V. Spinolo.

17-05: *A mathematical model for piracy control through police response*, G.M. Coclite, M. Garavelllo, L.V. Spinolo.

17-06: *Uncertainty Quantification of geochemical and mechanical compaction in layered sedimentary basins*, I. Colombo, F. Nobile, G. Porta, A. Scotti, L. Tamellini.

17-07: *VVS medical workflows: definition of a static workflow for part-based annotation of wrist bones & web service oriented architecture for executable workflows*, M. Pitikakis, F. Giannini.

17-08: *Computational Methods for the Morphological Analysis and Annotation of Segmented 3D Medical Data*, G. Patanè, F. Giannini, M. Attene.

17-09: *Applying Functional Principal Components to Structural Topology Optimization,* G. Alaimo, F. Auricchio, I. Bianchini, E. Lanzarone.